Effect of critical latitude and seasonal stratification on tidal current profiles along Ronne Ice Front, Antarctica

Keith Makinson,[1] Michael Schröder,[2] and Svein Østerhus[3]

Received 18 May 2005; revised 2 December 2005; accepted 27 December 2005; published 30 March 2006.

[1] The ice front region of Ronne Ice Shelf lies near the critical latitude of the semidiurnal M_2 tide, the principal tidal constituent in the southern Weddell Sea. Here the Coriolis frequency almost equals the M_2 tidal frequency, resulting in a strong dependence of the M_2 tidal currents on depth and stratification and a boundary layer that can occupy the entire water column. Using data from four long-term moorings along Ronne Ice Front, we confirm the presence of strongly depth-dependent semidiurnal tidal currents and their sensitivity to changes in stratification. The time series show dramatic seasonal changes in tidal current profiles and significant interannual variability. During periods of stratification, the amplitude of the semidiurnal tides in the mid–water column shows a twofold increase and, despite being several kilometers offshore from the ice front, the tidal currents clearly show a second boundary layer originating from the adjacent ice shelf base. Together, these two boundary layers occupy most of the water column, up to 600 m deep, until intense sea ice formation and the production of High-Salinity Shelf Water erodes the vertical stratification. During winter when homogeneous conditions prevail, a single bottom boundary layer occupies the entire water column at some locations. This strong seasonality and sensitivity of the M_2 tidal current to stratification highlights the difficulties of interpreting current data from short-term moorings while demonstrating that it is the best indicator for characterizing changes in stratification after direct observations of density variations.

Citation: Makinson, K., M. Schröder, and S. Østerhus (2006), Effect of critical latitude and seasonal stratification on tidal current profiles along Ronne Ice Front, Antarctica, *J. Geophys. Res.*, *111*, C03022, doi:10.1029/2005JC003062.

1. Introduction

[2] Winds blowing from Ronne Ice Shelf and tidal divergence maintain a coastal polynya along Ronne Ice Front in the southern Weddell Sea throughout much of the year [*Foldvik et al.*, 2001; *Renfrew et al.*, 2002]. During the summer melt season, solar radiation enlarges the polynya and warms the surface waters. In wintertime however, the coastal polynya is the focus of intense heat loss as relatively warm water is exposed to the cold atmosphere, causing the seawater to cool to its surface freezing point, with further heat loss resulting in sea ice production. Sustained sea ice production is maintained as newly formed sea ice is transported northward away from the polynya by offshore winds. Production rates are 1 or 2 orders of magnitude higher than for the surrounding sea, which is already covered with ice. Hence about 6% of the entire sea ice production is focused within a polynya that makes up only 0.13% of the Weddell Sea [*Renfrew et al.*, 2002]. The associated production of High-Salinity Shelf Water (HSSW) is likely to be equally intense, resulting in convective overturning of the entire underlying water column during winter [*Foldvik et al.*, 2001; *Nicholls et al.*, 2003]. At the ice front, this HSSW has been observed to flow along and toward the ice front [*Foldvik et al.*, 2001; *Woodgate et al.*, 1998] and drain deep into the sub–ice shelf cavity [*Nicholls and Makinson*, 1998; *Nicholls et al.*, 2001]. Interactions with the base of Filchner-Ronne Ice Shelf (FRIS) convert HSSW into Ice Shelf Water (ISW), a water mass that is fresher, and by definition, colder than the surface freezing point. Ultimately, this water reaches the northerly point of Filchner Depression where it overflows the continental shelf break [*Nicholls et al.*, 2001], making a significant contribution to the production of Weddell Sea Bottom Water [*Foldvik et al.*, 2004], a precursor of Antarctic Bottom Water.

[3] The application of two-dimensional barotropic tidal models to the southern Weddell Sea [*Makinson and Nicholls*, 1999; *Robertson et al.*, 1998] and observations offshore of Ronne Ice Front [*Foldvik et al.*, 2001; *Woodgate et al.*, 1998] show this region to be tidally active, with tidal currents of 20–40 cm s^{-1} during spring tides with excursions of 4–8 km [*Makinson*, 2002b]. In addition, the northwest corner of the Ronne Ice Front region lies near the critical latitude (λ_{crit}) of the M_2 tidal constituent at 74°28′18″S. Here the Coriolis

[1]British Antarctic Survey, Natural Environment Research Council, Cambridge, UK.
[2]Alfred-Wegener-Institut für Polar- und Meeresforschung, Bremerhaven, Germany.
[3]Bjerknes Centre for Climate Research, Geophysical Institute, University of Bergen, Bergen, Norway.

0148-0227/06/2005JC003062$09.00

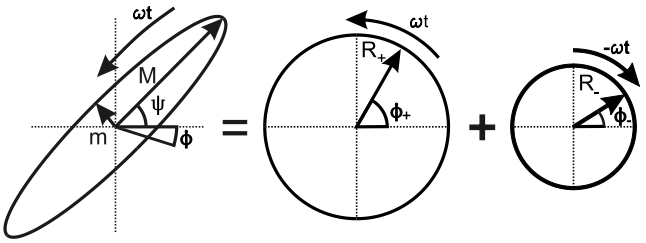

Figure 1. A tidal current vector, rotating at frequency (ω), traces out an ellipse that is described by four basic parameters: semi-major (M) and semiminor (m) axes, orientation (ψ) and phase angle (ϕ) or, alternatively, the sum of two counterrotating vectors with amplitudes R_+ and R_- and phases ϕ_+ and ϕ_-.

frequency equals the tidal frequency and semidiurnal tidal currents near λ_{crit} are known to have a strong depth dependence [*Foldvik et al.*, 2001; *Foldvik et al.*, 1990] and changes in stratification are likely to significantly affect the tidal current profile [*Makinson*, 2002a]. In order to study the vertical structure of tidal currents, various analytical solutions and numerical models have been successfully applied to continental shelf seas with a homogenous water column [e.g., *Furevik and Foldvik*, 1996; *Nøst*, 1994; *Simpson and Sharples*, 1994; *Soulsby*, 1983]. Where the water column is stratified and close to λ_{crit}, numerical modeling has shown that stratification significantly affects how the polarization of the tidal current ellipse varies with depth [*Makinson*, 2002a]. Using a one-dimensional turbulence closure model and separating the tidal constituents into rotary components, *Makinson* [2002a] modeled tidal current profiles beneath FRIS to determine the effects of polarization on vertical mixing. Polarization, $P = m/M$, was used to define the shape and sense of rotation of a tidal current ellipse in terms of the semimajor (M) and semiminor (m) axes (Figure 1). The model showed that predominantly anticlockwise tidal currents ($P > 0$) produce significantly higher levels of mixing than clockwise tidal currents ($P < 0$). This effect was accounted for by decomposing the elliptical tidal current vector into purely anticlockwise (R_+) and clockwise (R_-) components and considering their respective frictional boundary layers. The two, constant magnitude, rotary velocity components rotate at the tidal frequency, and each has a characteristic frictional boundary layer thickness, δ_+ and δ_-, given by *Prandle* [1982].

$$\delta_+ \approx \left(\frac{2K_M}{|\omega + f|}\right)^{1/2} \tag{1a}$$

$$\delta_- \approx \left(\frac{2K_M}{|\omega - f|}\right)^{1/2}, \tag{1b}$$

where K_M is the vertical eddy viscosity, f is the Coriolis parameter and ω is the frequency of the tidal oscillation. Therefore, in the Southern Hemisphere, tidal currents with more positive polarizations (anticlockwise rotation) have larger boundary layers.

[4] At high southern latitudes, the boundary layer of R_+ for semidiurnal tides is much larger than that of the corresponding R_- component, as $|\omega + f|$ tends to zero at λ_{crit}. At this latitude the tidal frequency equals the Coriolis or inertial frequency, $\omega = |f| = 2\Omega \sin \lambda_{crit}$, where the Earth's angular velocity $\Omega = 7.2921151 \times 10^{-5}$ rad s^{-1}. Beneath Ronne Ice Shelf, *Makinson* [2002a] showed that the combined upper and lower boundary layers could occupy the entire water column, as either λ_{crit} was approached or the tidal amplitude increased. These thicker boundary layers produce less intense shear near a boundary but extend the shear over a larger thickness of the water column, near λ_{crit}; effectively redistributing and modifying the profile of vertical mixing. At polar latitudes, this effect applies to semidiurnal tides. For diurnal tides at polar latitudes, $|f|$ is almost twice as large as ω, hence they do not exhibit these large differences in the rotary boundary layers of R_+ and R_-, and are generally barotropic [*Robertson*, 2005b].

[5] The boundary layer thickness is further complicated by stratification, which can dramatically affect the shape of the R_+ tidal current profile, while the R_- component remains unaffected [*Makinson*, 2002a]. Stratification suppresses turbulent motions and inhibits the transfer of momentum, giving a reduced boundary layer thickness compared with the homogenous case, and a reduced eddy viscosity, particularly in the vicinity of a pycnocline [*Souza and Simpson*, 1996]. Both observations and numerical modeling beneath fixed ice cover have found that the water column in the vicinity of the pycnocline becomes decoupled from the boundary layers at the seabed and ice base. This decoupling of the water column around the pycnocline results in a significant increase in the tidal current as it approaches or attains its free stream velocity [*Makinson*, 2002a; *Prinsenberg and Bennett*, 1989].

[6] One of the first comprehensive studies of seasonal changes in tidal currents was presented by *Howarth* [1998], who showed the significant differences in tidal current structure between the well-mixed winter conditions and stratified summer conditions in the North Sea. Here, the surface layer above the pycnocline became decoupled from the bottom boundary layer during summer months; with the orientation of bottom currents rotated 25° relative to the surface, and with their phase 30° (1 hour) in advance of the surface. In the southern Weddell Sea few long-term moorings have been deployed to enable studies of seasonal variations. However, *Foldvik et al.* [1990] considered seasonal changes in tidal currents from moorings at the continental shelf break, but found changes in both diurnal and semidiurnal tides and attributed these variations to the interaction of barotropic shelf waves with topography and a seasonal mean current. With the paucity of observational data, numerical models have been used more extensively in the southern Weddell Sea to study the effects of λ_{crit} and stratification. Although the focus of attention has been along the southern shelf break, the models show a bottom boundary layer up to 150 m thick close to λ_{crit}, with changes in stratification producing only small differences in tidal amplitude close to the pycnocline [*Pereira et al.*, 2002; *Robertson*, 2001b].

[7] Along Ronne Ice Front, previous observations of tidal currents have mainly been confined to short summer observations. However, four moorings with records greater

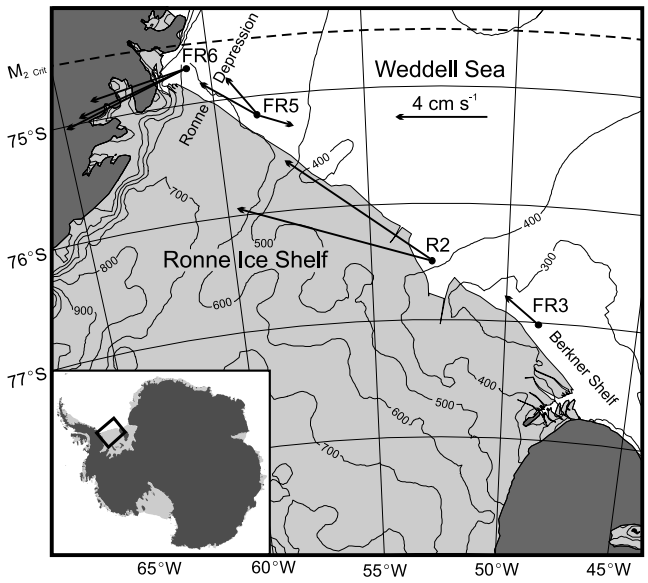

Figure 2. Map showing the ice front region of Ronne Ice Shelf. The locations of the ice front moorings are indicated together with arrows showing the time-averaged currents for each instrument. The contours indicate the bedrock depth below sea level, with a 100-m contour interval [*Vaughan et al.*, 1994], and the M_2 critical latitude is marked by the dashed line at 74°28′18″S.

than 1 year have been successfully recovered from the Ronne Ice Front coastal polynya [*Foldvik et al.*, 2001; *Woodgate et al.*, 1998] and form the basis of the work presented in this paper. With the exception of numerical modeling, the effects on observed tidal current profiles of seasonal changes in stratification and proximity to λ_{crit} have not been studied. The aim of this paper is to discuss the influence of λ_{crit} and changes in stratification, on tidal currents and their vertical profiles along Ronne Ice Front. In section 2 the moorings and other observational data are used to give an outline of the hydrography along Ronne Ice Front. Section 3 outlines how harmonic analysis is used to generate a time series of the positive and negative rotary tidal components for each of the major tidal constituents. These time series, together with temperature and salinity data from the moorings are then used in section 4 to show how the tidal components are influenced by seasonal stratification.

2. Ronne Ice Front: General Observations

[8] Almost all oceanographic observations along Ronne Ice Front have been made during the late austral summer, when light sea ice or open water allow ships to access the area. Wintertime observations are only possible through the deployment of long-term moorings, and Figure 2 shows the locations of four such moorings along Ronne Ice Front. All the moorings were deployed approximately 5–10 km from the ice front, which can advance at up to 1.9 km yr^{-1} [*Foldvik et al.*, 2001]. In total, nine instruments yielded records of between 1.2 and 2.5 years in length and Figure 3 shows their positions within the water column. The first long-term mooring, R2, was deployed in February 1993 roughly midway along Ronne Ice Front. R2 contained two current meters, each with temperature and conductivity sensors that remained operational until April 1994 [*Foldvik et al.*, 2001]. The other ice front moorings, one on Berkner Shelf (FR3) and two in Ronne Depression (FR5 and FR6), were deployed in early 1995 and remained operational until May 1997. Each of the current meters on the FR moorings had temperature sensors, with the shallowest instrument at FR6 and the instrument at FR3 also having a conductivity sensor

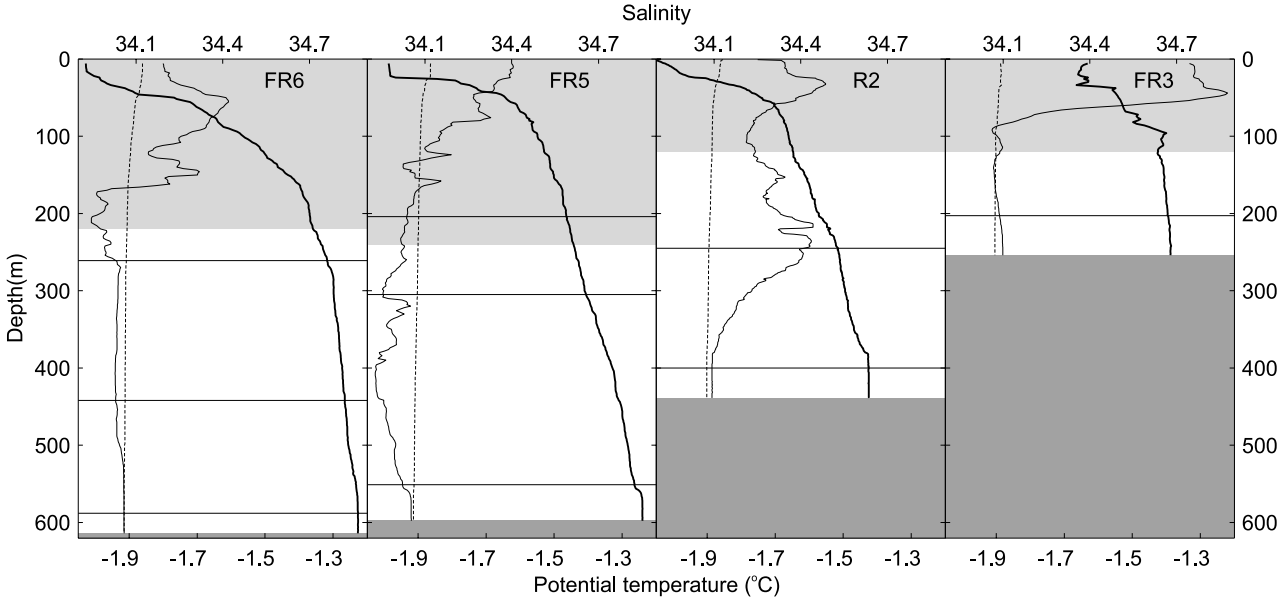

Figure 3. Vertical profiles of potential temperature (thin line), salinity (thick line), and surface freezing point (dashed line) close to each mooring location at the time of deployment. The light shaded area shows the part of the water column occupied by the adjacent ice shelf, and dark shading indicates the seabed. The thin horizontal lines show the depth of the moored instruments.

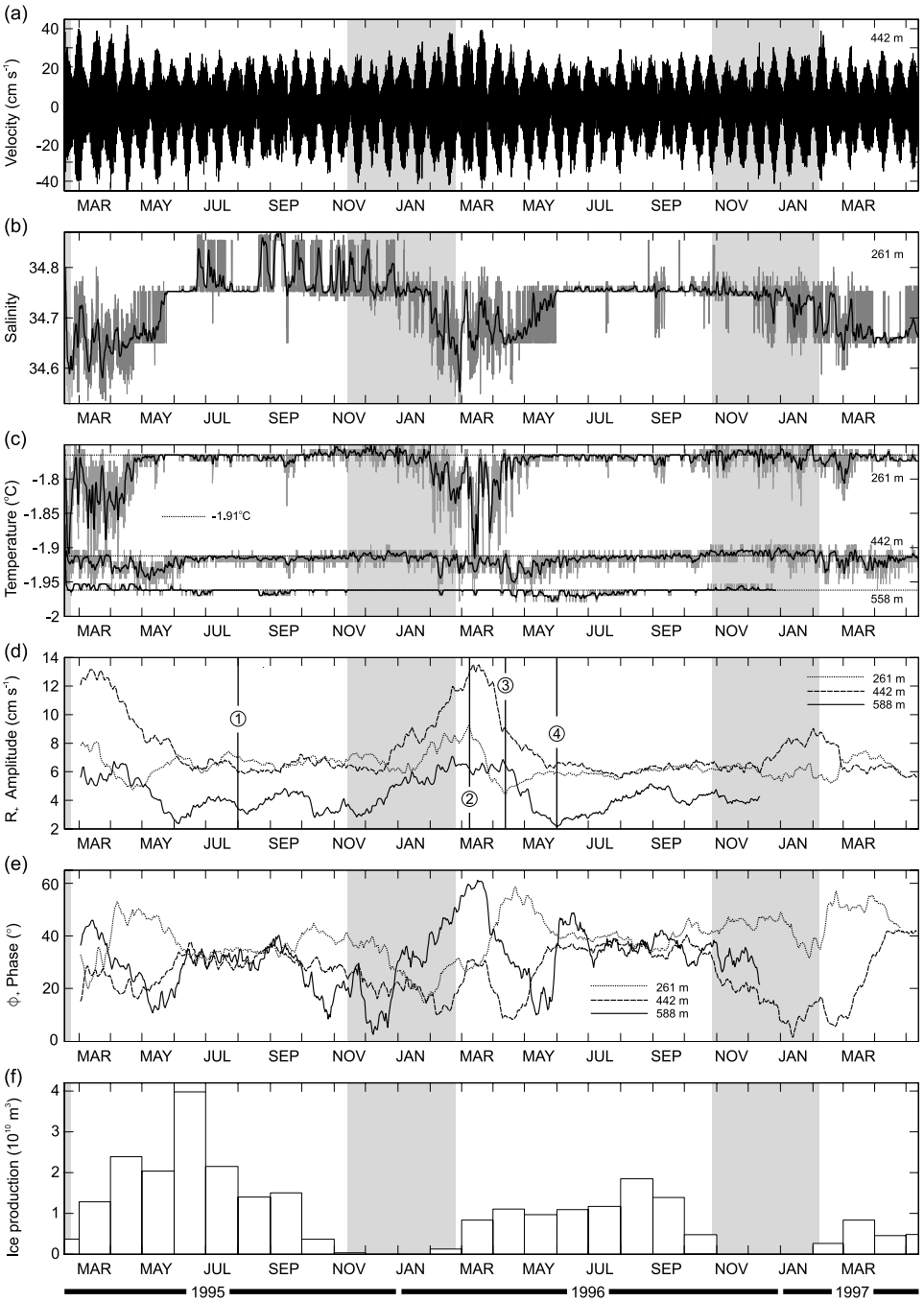

Figure 4. Time series data from mooring FR6. (a) High-pass-filtered (2-day) current component perpendicular to the ice front at 442 m. (b) Raw and daily averaged salinity time series data from the upper instrument at 261 m. (c) Raw and daily averaged potential temperature time series data. The data from 261 and 588 m have been offset by 0.15°C and −0.05°C, respectively, to improve clarity, and the dotted line shows the surface freezing temperature of −1.91°C. (d) Time series of the anticlockwise rotary component amplitude (R_+) for the M_2 tidal constituent. The numbered vertical lines show when R_+ observations are used for the vertical profiles in Figure 6. (e) Time series of the anticlockwise rotary component phase (ϕ_+) for the M_2 tidal constituent. At 558 m, ϕ_+ has been offset by 60°. (f) Bar chart of sea ice production in the coastal polynya along Ronne Ice Front for each month of the mooring record. The shaded areas in each plot show the summer melting season [*Renfrew et al.*, 2002].

[*Woodgate et al.*, 1998]. However, the resolution of conductivity data from the moorings is only 0.072 mS cm^{-1}, whereas the temperature resolution is 0.008°C, resulting in a derived salinity resolution of only 0.1. This poor resolution is most apparent during winter months, when the water column remains close to the surface freezing point and the salinity tends to only a few values, even after smoothing the data to obtain daily averages. Clear examples of this

Table 1. Details of the Instrument Records From the Four Long-Term Moorings From the Ice Front Region of Ronne Ice Shelf

Mooring	Position	Water Depth, m	Ice shelf Draft, m	Instrument Depth, m	Start Date	Duration, days	Sensors	Distance from M_2 φ_{crit}, km
FR6	74°, 42.3′S	613	220	261	16 Feb 1995	816	speed, direction, *T, C, P*	26
	60°, 48.6′W			442	16 Feb 1995	830	speed, direction, *T*	
				588	16 Feb 1995	679	speed, direction, *T*	
FR5	75°, 09.8′S	601	240	204	15 Feb 1995	816	speed, direction, *T, P*	77
	58°, 43.6′W			305	15 Feb 1995	830	speed, direction, *T, P*	
				551	29 Jun 1995	545	speed, direction, *T*	
R2	76°, 28.85′S	419	120	245	5 Feb 1993	435	speed, direction, *T, C*	223
	53°, 00.03′W			400	5 Feb 1993	435	speed, direction, *T, C*	
FR3	77°, 00.1′S	254	120	203	26 Jan 1995	837	speed, direction, *T, C*	281
	49°, 01.3′W							

effect are seen in the 1995 and 1996 winter salinity data (Figure 4b). However, increased water column variability during late summer and early winter, allows the smoothed data to reveal a more precise daily average, particularly for salinity. A summary of all the moorings is given in Table 1.

[9] At each mooring location, conductivity-temperature-depth (CTD) measurements were taken close to the time of deployment to provide a snapshot of the water column structure and a calibration for the moored instruments. Figure 3 shows the potential temperature, salinity and surface freezing point profiles from each location during late summer. All the profiles have fresher, warmer surface waters in the upper 50 m with maximum temperatures located at 30–50 m, with all but FR5 showing signs of surface cooling. At both FR5 and FR6, ISW occupies the water column between about 150 m and 550 m, with FR3 showing traces of ISW at around 100 m and 150 m. However, at R2, the central water column between 150 m and 280 m is dominated by Modified Weddell Deep Water (MWDW) ($T > -1.7°C$, $S < 34.6$), the product of mixing between Winter Water and Weddell Deep Water that has penetrated across the continental shelf. Close to the seabed at each mooring, the HSSW has a potential temperature either at or close to the surface freezing point, reflecting the conditions present throughout the water column during wintertime convection, with the highest salinities reaching over 34.86 in the western Ronne Depression. At the time of each deployment, a bottom mixed layer ranging from 25–55 m is present and probably results from tidal mixing. The density of cold polar waters is dictated by salinity and Figure 3 shows that away from the surface waters the water column has relatively weak stratification, with buoyancy frequencies typically ranging from 0.0015 to 0.0025 s^{-1}.

[10] Using a combination of satellite observations, meteorological data and simple physical models, *Renfrew et al.* [2002] evaluated the heat fluxes, sea ice production and the timing of the melting and freezing seasons along Ronne Ice Front for the period from 1992 to 1998. This 7-year period encompasses the time when the ice front moorings were operational. Typically, an average summer melting season begins 6 November, lasts until 19 February, and is followed by a 257-day winter freezing season during which time the coastal polynya produces an average of 24 m of sea ice [*Renfrew et al.*, 2002]. This annual sea ice production and associated expulsion of brine is clearly recorded at all four ice front moorings by the presence of HSSW throughout the water column, with high salinities during late winter and water column temperatures at or close to the surface freezing point. There is a lag between the onset of winter freezing and the appearance of HSSW at the depth of each instrument as illustrated in Figure 4. Here, the temperature at FR6 (261 m) reaches the surface freezing point in early April about 6 weeks after the onset of winter freezing, and is closely followed by a response in salinity. Both temperature and salinity show a progressive increase until a wintertime plateau is reached, characteristics that have been observed during winter in the Okhotsk Sea for example [*Shcherbina et al.*, 2003]. Deeper within the water column at FR6 (442 m) the temperature response lags by a further 6 weeks as the HSSW penetrates deeper into the water column. The intensity of sea ice production at the start of the freezing season is also reflected in the salinity record. In May 1995 the increase of 0.08 in salinity to wintertime values occurs over a 2-week period whereas in 1996 the same transition took almost 6 weeks as a result of the weaker sea ice production (Figure 4f). The higher sea ice production during 1995, particularly during June, is followed by the highest observed salinities throughout the record. However, during the summer and early winter, seasonal stratification results from the presence of lower salinity water masses, such as ISW or MWDW, that are advected along the ice front [*Foldvik et al.*, 2001; *Woodgate et al.*, 1998]. This mean flow along the ice front exhibits seasonal and interannual variability but is generally toward the northwest, parallel to the ice front, with instruments at FR6 and R2 showing a significant component of flow directed beneath the ice shelf (Figure 1).

[11] Clearly, the Ronne Ice Front region is dominated by strong seasonal signals in the meteorology that are reflected in the rates of sea ice production, HSSW formation and therefore the water column structure. With recent modeling work suggesting that semidiurnal tides, particularly M_2, are likely to exhibit strong seasonal characteristics [*Makinson*, 2002a], we analyze the ice front mooring data and use them to describe the tidal current profiles and any seasonal variations.

3. Analysis

[12] A harmonic analysis of the current meter data yields the amplitude and phase of the east-west and north-south velocity components for each tidal constituent. These four parameters define the tidal ellipse traced out by the tip of the current vector (**V**) for each component, and can be used to give the amplitudes of the semimajor (M) and semiminor (m) axis, angle of the inclination or ellipse orientation (ψ), and Greenwich phase angle (ϕ) (Figure 1). Alternatively, the

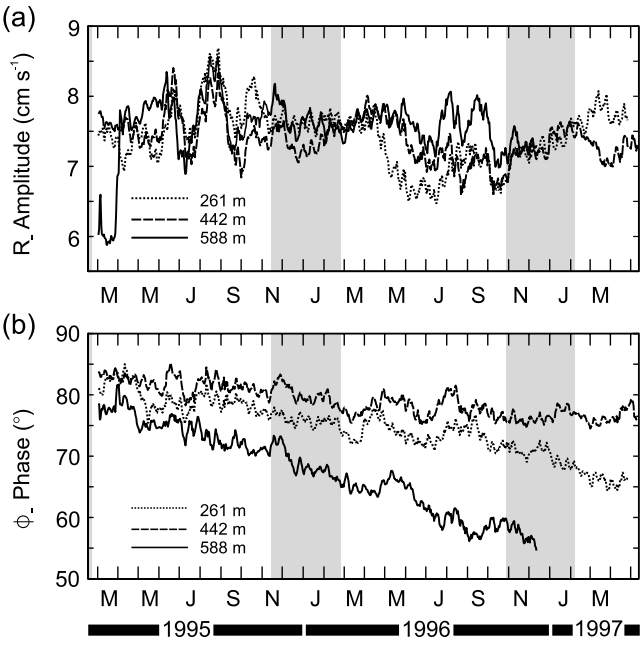

Figure 5. Time series data of the M_2 clockwise tidal component at mooring FR6 showing (a) the amplitude of R_- and (b) its phase (ϕ_-). The shaded areas in each plot indicate the summer melting season [*Renfrew et al.*, 2002].

ellipse velocity vector can be represented by the sum of two corotating vectors

$$\mathbf{V}(t) = R_+ \exp\big(i(\phi_+ + \omega t)\big) + R_- \exp(-i(\phi_- - \omega t)), \quad (2)$$

where t is time, ω is the tidal frequency, R_+ and R_- are the amplitudes of the positive and negative rotary components, and ϕ_+ and ϕ_- are the corresponding phases. From these parameters the semimajor and semiminor axes of the ellipse are

$$M = R_+ + R_- \quad (3)$$

$$m = R_+ - R_-, \quad (4)$$

and the orientation of the semimajor axis relative to east and Greenwich phase angle is

$$\psi = \big(\phi_+ + \phi_-\big)/2 \quad (5)$$

$$\phi = \big(\phi_+ - \phi_-\big)/2. \quad (6)$$

[13] The sign of the semiminor axis represents the direction of rotation of the tidal ellipse, with polarization, which ranges between ±1, describing both the shape and sense of rotation. If positive, the current rotates anticlockwise; if negative, the current rotates clockwise. Close to λ_{crit} or where large boundary layers occur, the ellipse polarization in the Southern Hemisphere can become increasingly negative toward the seabed because of the strong depth dependence of R_+, possibly resulting in a change in the sense of rotation. This characteristic has been observed for M_2 in the southern Weddell Sea close to the shelf break [*Foldvik et al.*, 1990] and at the ice front mooring, R2 [*Foldvik et al.*, 2001]. *Woodgate et al.* [1998] analyzed the entire time series at FR5 and FR6 and showed that the semidiurnal tides maintain clockwise rotation below the draft of the nearby ice shelf. At FR6, the lowermost instrument has more negative polarization than those above, indicating that it is located within the bottom boundary layer. However, FR5 shows no such characteristic, with the polarization becoming gradually more positive toward the seabed, suggesting that only a small bottom boundary layer is present below the deepest instrument. FR3 shows anticlockwise rotation, but having only a single current meter it is not possible to determine if the polarization is depth-dependent.

[14] In order to identify any seasonal changes in the tidal currents it is necessary to analyze short sections of the current meter time series. The M_2 tide is the largest tide in the region and $\lambda_{crit}(M_2)$ at 74°28′180″S, is closest to Ronne Ice Front and therefore of primary interest. Of the principal tides with frequencies near that of M_2, N_2 is closest, followed by S_2, with $\lambda_{crit}(N_2)$ at 70°58′47″S and $\lambda_{crit}(S_2)$ at 85°45′54″S. In order to separate these tides, the initial 27.6-day section of a current meter record was harmonically analyzed, separating a total of six tidal constituents (Q_1, O_1, K_1, N_2, M_2, and S_2) [*Foreman*, 1977]. This analysis was repeated by moving the 27.6-day window forward in 1-day steps until the end of the record was reached, creating a time series of the rotary components for each tidal constituent.

4. Tidal Variability

[15] Using data from FR6 together with tidal analysis and sea ice data, we give a comprehensive description of the processes that contribute to the tidal variability at this ice front mooring. Building on these results, we then describe the tidal currents at the three remaining moorings, while emphasizing the unique tidal features at each location.

4.1. Mooring FR6

[16] The nearest ice front mooring to $\lambda_{crit}(M_2)$ is FR6, only 26 km to the south and close to the northwest corner of Ronne Ice Shelf. The results of the decomposition of the M_2 tidal currents into rotary components for each instrument are shown in Figure 4, which gives the amplitude of R_+ and its phase, ϕ_+. The most striking feature is the strong seasonal signal in both R_+ and ϕ_+, together with some interannual variability, however, neither R_- nor ϕ_- contain significant seasonal signals (Figure 5). The rest of Figure 4 shows the seasonal signals in temperature, salinity, and monthly sea ice production [*Renfrew et al.*, 2002] within the ice front polynya. These seasonal changes in stratification, together with the proximity of $\lambda_{crit}(M_2)$, result in R_+ (M_2) at 442 m exhibiting a twofold increase during summer months with swings of up to 50° in ϕ_+ at 261 m. Furthermore, the changes in stratification can also result in twofold increases in R_+ (S_2) and R_+ (N_2) at FR6 (442 m) [*Makinson*, 2002b; *Makinson and Schröder*, 2004]. Although the critical latitudes of S_2 and N_2 are remote from FR6, harmonic tidal analysis of the winter periods indicates that these semidiurnal tides have large R_+ boundary layers during winter as predicted by simple boundary layer theory (1a, 1b). The boundary layer of R_+ (M_2) achieves about 50% of its free stream amplitude 25 m above the seabed (588 m) and can extend beyond the instrument at 442 m (profile 1, Figure 6), while the boundary layers of R_+ (S_2) and R_+ (N_2) exhibit similar characteristics (not shown).

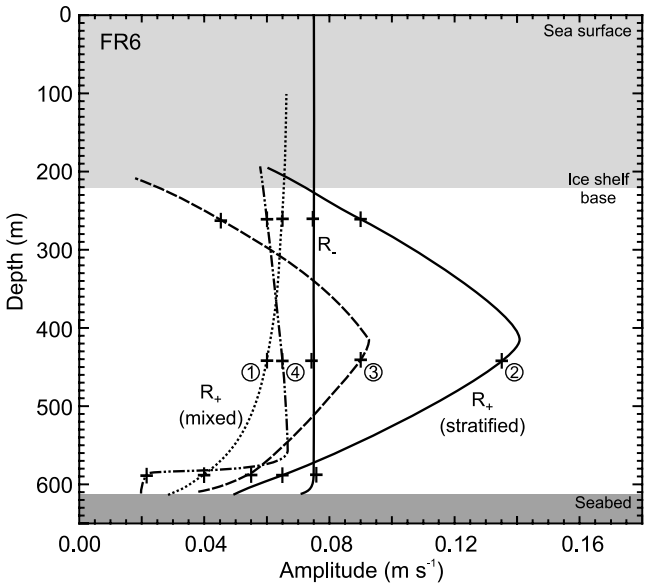

Figure 6. Depth variations of the clockwise (R_-) and anticlockwise (R_+) tidal current components for M_2 at mooring FR6. The profile numbers correspond to the numbered vertical lines in Figure 4d, and the crosses are the current meter measurements from those times. The profile lines indicate the conceptual vertical R_+ current profiles for well-mixed (profile 1) and stratified (profile 2) conditions. Profiles 3 and 4 occur during transitional conditions, with R_- remaining unaffected. The light shading indicates the portion of water column occupied by the nearby ice shelf, and the dark shading indicates the seabed.

Similar bottom boundary layer characteristics for the semidiurnal tides also occur at mooring R2 during wintertime and the occurrence of large R_+ boundary layers (>100 m), which could respond to changes in stratification, are also observed at other high-latitude sites located over 20° (2200 km) away from λ_{crit}. Close to the M_2 λ_{crit} and the continental shelf slope of the southern Weddell Sea, *Foldvik et al.* [1990] observed the R_+ (S_2) boundary layer extending through the lower 100 m of water column. In arctic Canada, sites in Hudson Bay (63°N) and Peel Sound (73.5°N) also show the S_2 boundary layer, up to 200 m thick, occupying almost the entire water column [*Prinsenberg and Bennett*, 1989]. However, no studies regarding the influence of seasonal stratification on these tidal current profiles were undertaken, although simple boundary layer theory (equations (1a) and (1b)) predicts that the semidiurnal tides at high latitudes will remain sensitive to changes in K_M, and therefore stratification. Conversely, the clockwise tidal component of the semidiurnal tides and both components of the diurnal tides remain unaffected by the seasonal changes in stratification.

[17] At FR6, the seasonality of the semidiurnal tides increases the peak spring tidal current in the mid–water column (442 m) from around ±25 cm s^{-1} during midwinter, to almost ±40 cm s^{-1} during late summer and early winter, an increase of around 50% (Figure 4a), while the diurnal tides exhibit no seasonality. The changes in ϕ_+ for the other semidiurnal tides can also be over 40°, equivalent to 20° in ellipse orientation, which at FR6 is typically 55° during winter.

[18] Another potential source of seasonal depth-dependent tidal variability could result from the affect of stratification and the propagation of internal tides. Generated over regions of steep topography, such as continental shelf slopes or an ice front, internal tides can result in strong vertical shears in the horizontal velocities. However, linear internal wave theory for a continuously stratified fluid predicts that internal tides will neither be generated nor propagate poleward of the critical latitude (a more extensive explanation of the relevant linear internal wave theory is given by *Robertson* [2001a]). Here the critical latitude acts as a turning latitude, preventing internal tides from propagating farther poleward although the critical latitude and turning latitude do not always coincide. Using equation 10.26 from *LeBlond and Mysak* [1978] and assuming a mean buoyancy frequency of 0.002 s^{-1} for the region around FR6, the M_2 turning latitude is less than 5 km to the south of the critical latitude. Therefore the turning latitude remains remote from FR6 and the other ice front moorings, while the internal tide energy poleward of the critical latitude is damped exponentially, potentially introducing some residual internal wave energy to the more northern ice front observations.

[19] While internal tides are not expected in a continuously stratified water column, *Robertson* [2005a] and *Robertson et al.* [2003] found that internal tides can exist poleward of the critical latitude at the front of and beneath Ross Ice Shelf, because of the hydrographic conditions within the cavity. Beneath the ice shelf the water column responded as a simple two-layer system, particularly deep within the cavity and to a lesser degree at the ice front, potentially influencing tidal observations at ice front moorings. Applying the same model to the Weddell Sea and imposing a similarly simple layered water column beneath FRIS, resulted in no significant internal wave response within the cavity [*Robertson*, 2005b]. However, *Robertson* [2005b] noted that diurnal continental shelf waves generated over regions of steep topography, particularly over the continental shelf edge, amplified the baroclinic semidiurnal tides. Along Ronne Ice Front, less vigorous continental shelf waves were observed within the model but no significant semidiurnal response was reported. Clearly, these processes could contribute to the observed seasonal variability, but the influence of stratification on semidiurnal tidal boundary layers appears to be the primary source of seasonal tidal variability along Ronne Ice Front.

[20] One feature common to all the ice front data is an overall decrease in M_2 ϕ_- of 8°–18° yr^{-1} in the instruments nearest the seabed and a decrease of 4°–7° yr^{-1} higher in the water column. An example of this, Figure 5b shows the decrease in M_2 ϕ_- for mooring FR6. In addition, there is a similar annual increase in M_2 ϕ_+; hence the average ellipse orientation generally remains fixed (see equation (5)). Other semidiurnal and diurnal tides show similar phase changes, which are presumably the result of the ice front advancing toward the moorings. Using the tidal models of *Makinson and Nicholls* [1999] and *Padman et al.* [2002] and converting the tidal constituents in rotary vectors, the data show that ϕ_+ and ϕ_- change significantly in the region of Ronne Ice Front. However, the magnitude of spatial gradients is

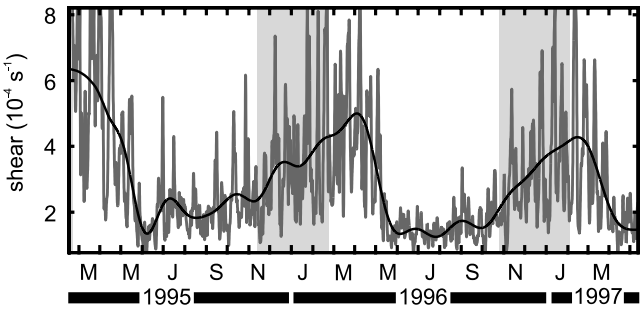

Figure 7. Velocity shear time series at FR6 between the current meters at 261 and 442 m for the 0–15 hour frequency band. The data have been low-pass filtered with a 2-day cutoff to reduce signal noise. Applying a low-pass filter (60 day), the seasonal signal is highlighted by the heavy line, and the shaded areas show the summer melting season [*Renfrew et al.*, 2002].

underestimated, probably because the present models only have 7–10 km grid spacing.

[21] With three current meters at FR6, vertical profiles of the rotary components can be created for various times throughout the year. On the basis of the analysis of the rotary components at each instrument, the crosses in Figure 6 show the observed R_+ for the times indicated in Figure 4, but with almost no knowledge of the water column structure, suggesting R_+ profiles is difficult. However, *Makinson* [2002a] applied a 1-D vertical mixing model to the water column beneath FRIS to examined the effect of critical latitude and stratification on boundary layer structure and vertical mixing. The model showed that stratification significantly affects the R_+ (M_2) tidal current profile due, in large part, to the proximity of $\lambda_{crit}(M_2)$, thus providing insight into how changes in stratification influence the boundary layer structure close to $\lambda_{crit}(M_2)$. On the basis of both observations from the Arctic [*Prinsenberg and Bennett*, 1989] and qualitatively on profiles modeled by *Makinson* [2002a], the R_+ profiles in Figure 6 are conceptual curves used to show the evolution of R_+ through the seasons.

[22] The mooring data in Figure 4 show that by late winter the potential temperature reaches a plateau as HSSW occupies the entire water column and little or no stratification is likely to be present, particularly during 1995 when sea ice production was over 70% higher than in 1996. During this winter period, from June to September 1995, the water temperature together with R_+ and ϕ_+ remain relatively stable, suggesting a well-mixed water column. At times the frictional bottom boundary layer at FR6 extends beyond the instrument at 442 m, over 170 m from the seabed, as a result of the proximity to $\lambda_{crit}(M_2)$ (profile 1, Figure 6), with R_- having an almost uniform profile. After the end of September, the upper water column warms slightly and the earlier peaks in salinity begin to decrease as sea ice formation declines throughout October, with almost no sea ice formed in November (Figure 4). There is no obvious response to these changes in R_+, but ϕ_+, which has been stable throughout the latter half of winter, diverges from its wintertime values during October as the supply of HSSW from sea ice formation diminishes and the water column begins to stratify. Through December and January R_+ increases at each of the instruments. By early February, a reduction in temperature and salinity at the upper instrument indicates the arrival of ISW with a correspondingly large increase of R_+. However, through this summer period and despite FR6 being offshore, profile 2 in Figure 6 is similar to modeled [*Makinson*, 2002a] and observed [*Prinsenberg and Bennett*, 1989] R_+ current profiles found beneath fast ice cover. It appears that during summer stratification, the presence of the ice shelf base influences tidal currents several kilometers offshore, with R_+ decreasing in the upper half of the water column because of a second boundary layer originating from the adjacent ice shelf base, while R_- remains unaffected. The relatively strong stratification in the upper water column (Figure 3) decouples the water column below the ice shelf draft from that above in terms of the semidiurnal anticlockwise components. This decoupling allows a boundary layer, generated by the ice shelf base and extending downward, to be present some distance from the ice front. Also, the decoupling of the upper water column effectively creates a blockage of flow above the ice shelf base for R_+ and in the following section, this effect is clearly seen at FR5 where one instrument is located above the ice shelf draft. However, within the limitations of these sparse observations, the depth-averaged tidal current does not appear to change appreciably with the seasons. By ignoring the fluctuations in ϕ_+ and assuming the depth averaged R_+ remains similar throughout the year, the averaged R_+ below the draft of the ice shelf, will increase by about 50% during periods of stratification. This increase in R_+ accounts for some of the seasonality; however, it is the proximity of the adjacent ice shelf base and the critical latitude that cause the development of the two large boundary layers which extend to occupy the entire water column below the draft of the ice shelf further amplifying R_+ in the mid–water column (Figure 6).

[23] The development of this mid–water column boundary layer originating from the ice shelf base is clearly illustrated by the semidiurnal tidal shear between the current meters at 261 m and 442 m (Figure 7). The velocity data were high-pass filtered (15 hours) before the shear was calculated and smoothed. Inclusion of the diurnal tides, which are principally barotropic and unaffected by stratification, would provide a small additional background shear of around 0.6×10^{-4} s^{-1} to the semidiurnal tidal shear shown in Figure 7. During the height of the winter freezing season, the semidiurnal tides are more barotropic and the shear between 261 m and 442 m has a minimal plateau. In the latter part of the freezing season however, sea ice formation declines and the water column begins to stratify, reducing momentum transport, and allowing shear to develop. Throughout the remainder of the summer melting season and into early winter, the shear increases almost linearly (Figure 7) as the stratification continues to increase. The response of the semidiurnal tides to these changes in stratification is initially confined to ϕ_+ when stratification and shear between 261 m and 442 m are weakest. As stratification continues to increase with the arrival of ISW, R_+ responds and amplitudes increase, ultimately reaching a maximum during March (Figure 4).

[24] With no rigid surface to maintain the mid–water column boundary layer, it will presumably diffuse and dissipate with distance away from the ice front. However,

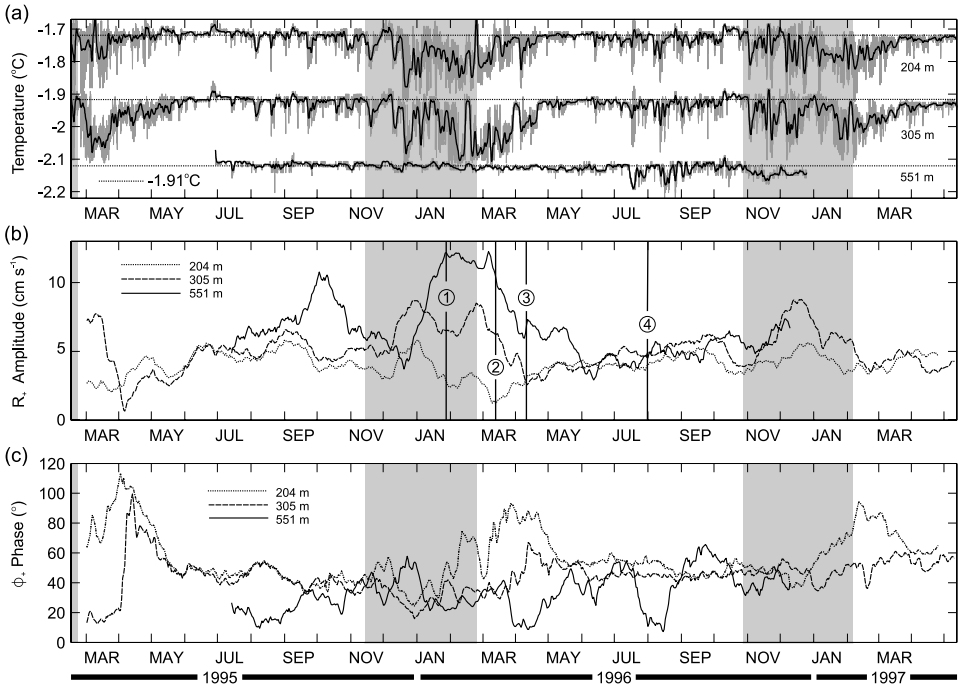

Figure 8. Time series data from mooring FR5. (a) Raw and daily averaged potential temperature time series data. The data from 204 and 551 m have been offset by 0.2°C and −0.2°C, respectively, and the dotted line shows the surface freezing temperature of −1.91°C. (b) Time series of the anticlockwise rotary component (R_+) for the M_2 tidal constituent. The numbered vertical lines show when R_+ observations are used for the vertical profiles in Figure 9. (c) Time series of the M_2 ϕ_+; at 551 m, ϕ_+ has been offset by 60°. The shaded areas in each plot show the summer melting season [*Renfrew et al.*, 2002].

it is unclear how far north the mid−water column boundary layer extends beyond the ice front in the absence of additional observations. Nevertheless, using a three dimensional model to investigate tidal mixing in the southern Weddell Sea, *Pereira et al.* [2002] show the major axis of the M_2 tidal ellipse remaining at a maximum in the mid−water column over 100 km from Ronne Ice Front. Although the enhanced mid−water column major axis is much smaller than observed at FR6, and is reliant on the stratification prescribed in the model; the model results suggest that the ice front influences the structure of the M_2 tidal currents many tens of kilometers to the north of Ronne Ice Shelf.

[25] Through February 1996 and into early March, R_+ continues to increase with increasing stratification, as the two boundary layers develop and occupy the entire water column below the ice shelf draft. The peaks in R_+ occur around mid-March (profile 2, Figure 6) about 20 days after the onset of the winter freezing season (25 February) [*Renfrew et al.*, 2002]. The subsequent rapid decline of R_+ signifies the switch from summer to winter conditions in the water column, as HSSW begins to form at the surface and descend into the water column.

[26] The decline of R_+ occurs soonest higher in the water column and takes place over a 2−4 week period. At 261 m, R_+ declines after mid-March and continues to a minimum in mid-April. At about the same time, the salinity begins to increase and the temperature plateaus (Figure 4). Temperatures close to the surface freezing point and an increasing salinity signifies the passage of the deepening pycnocline past this instrument. The strong stratification associated with this pycnocline suppresses turbulence and inhibits momentum transfer, causing the upper water column to become increasingly decoupled from that below. This decoupling allows the influence of the adjacent ice shelf boundary layer to be intensified, further decreasing R_+ at 261 m and 442 m (profile 3, Figure 6). The response of ϕ_+ to the arrival of the HSSW is signaled at 261 m by a 30° increase and a similar decrease at 588 m. At 442 m, the response of ϕ_+ from 30° to 10° follows the response at 588 m, suggesting that both of these instruments are within the lower boundary layer.

[27] By mid-May ϕ_+ has reverted to its wintertime value and the rapid decline of both R_+ at 442 m (Figure 4) and the tidal current shear between 261 m and 442 m has ceased (Figure 7). These events coincide with the arrival of HSSW at 442 m, as the temperature approaches a plateau and the pycnocline passes the instrument. With HSSW occupying the water column down to 442 m, the boundary layer generated by the ice shelf base is destroyed as R_+ becomes increasingly barotropic and the shear between 261 m and 442 m reverts to its minimal plateau (Figure 7). By the end of May, R_+ at 558 m reaches a minimum and ϕ_+ rapidly increases by 30° as the pycnocline reaches this instrument. Based qualitatively on the modeling work of *Makinson* [2002a], profile 4 in Figure 6 shows the high shear in R_+ across the pycnocline as it descends toward the seabed and reducing the boundary layer thickness. At about this time the salinity at 261 m attains its winter plateau, suggesting that the water column may be fully mixed. At the lowest instrument, however, the temperature does not finally plateau until July, when the R_+ and ϕ_+ finally recover to their winter values. Only during July through to September do

the instrument sensors and tidal parameters suggest that HSSW occupies the entire water column with little or no stratification present.

[28] During the summer period in early 1995, very similar changes in water column properties and tidal current response are observed, although absolute values and timings differ slightly from those in 1996. At each instrument, ϕ_+ changes rapidly as the minimum in R_+ is approached, coinciding with the arrival of the HSSW and the deepening pycnocline. During early 1997, however, both the temperature structure and tidal response differed significantly from the previous 2 years. Only relatively small changes R_+ are seen at 442 m although a strong response is observed in ϕ_+ as the water column stratifies, followed by a rapid recovery to the wintertime ϕ_+ during March and early April. These observations show that the tidal response to stratification occurs initially in ϕ_+, and that with increasing stratification a threshold is reached after which R_+ begins to respond. The interannual differences in stratification and the associated tidal current response could be influenced by the extent of the ice front polynya and its associated heat flux or sea ice production. In the summer of 1994–1995 the oceanic energy gain in the ice front polynya was 5.88×10^{19} J, reducing to 3.39×10^{19} and 1.66×10^{19} J in subsequent summers, with the winters of 1994 and 1996 having approximately 50% less sea ice production than 1995 [*Renfrew et al.*, 2002]. In the summer of 1996–1997, it is the combination of weak summer heat flux, preceded by low sea ice production that may be responsible for the weaker tidal response.

4.2. Mooring FR5

[29] Located in the eastern portion of Ronne Depression, close to the ice front, FR5 is 77 km south of $\lambda_{crit}(M_2)$. The decomposition of the tidal currents into rotary components for each instrument is shown in Figure 8. As at FR6, there are seasonal changes in the water column temperature that result from HSSW production in winter and advection of ISW during summer and early winter. Correspondingly, there is also a seasonal response in the tidal current amplitude and phase throughout the water column.

[30] One prominent feature during summertime stratification is that the largest observed R_+ (M_2) occurs not within the mid–water column, as at FR6, but at the deepest instrument, only 50 m from the seabed. Inspection of the CTD profile close to FR5 shows a well-mixed layer capped by a pycnocline just below the depth of the instrument (Figure 3). Presumably, this pycnocline inhibits the efficient transport of momentum, capping off any tidal bottom boundary layers and confining them below the lowest instrument while the boundary layer originating from the adjacent ice shelf base occupies the remainder of the water column below the ice shelf draft and the R_+ maximum closely tracks the pycnocline [*Makinson*, 2002a] (profile 1, Figure 9). These conditions are analogous to the inverted situation of a sub–ice shelf water column modeled by *Makinson* [2002a] where melting enabled the development of a pycnocline near the ice-ocean boundary, capping off this upper boundary layer. At the same time, strong shear was present in R_+ (M_2) across the pycnocline and the bottom boundary layer occupied the remainder of the water column [*Makinson*, 2002a]. Additionally at FR5, the instrument at 204 m is the only ice front instrument located above the draft of the nearby ice shelf and it clearly shows the decoupling of the upper water column from that below the ice shelf draft in terms of R_+ (M_2). Figure 8 illustrates that during periods of strong stratification R_+ at 204 m decreases, and that the decoupling of the upper water column effectively blocks the off the upper water column to semidiurnal anticlockwise components (Figure 9).

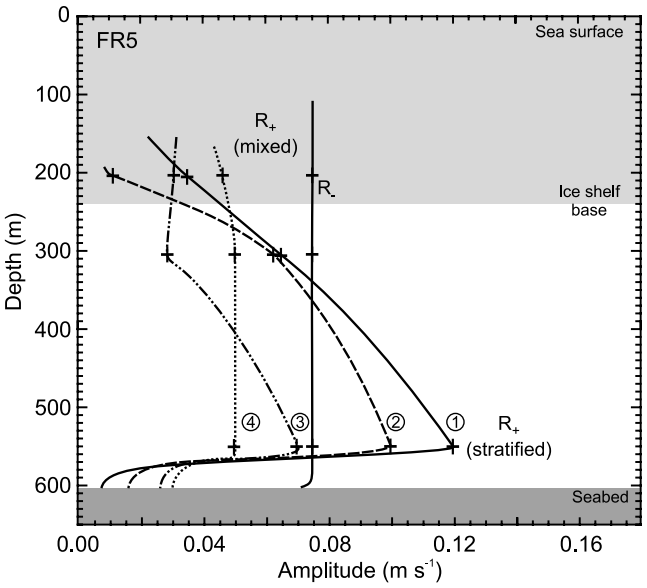

Figure 9. Depth variations of the clockwise (R_-) and anticlockwise (R_+) tidal current components for M_2 at mooring FR5. The profile numbers correspond to the numbered vertical lines in Figure 8b, and the crosses are the current meter measurements from those times. The profile lines indicate the conceptual vertical R_+ current profiles for stratified (profile 1) and well-mixed (profile 4) conditions. Profiles 2 and 3 occur during transitional conditions, with R_- remaining unaffected. The light shading indicates the portion of water column occupied by the nearby ice shelf, and the dark shading indicates the seabed.

[31] In common with FR6, the arrival of HSSW at an instrument is assumed to be signaled by a plateauing of the temperature, coinciding with a minimum in R_+ and a rapid change in the ϕ_+. Above the draft of the ice shelf, R_+ (204 m) in Figure 8 declines to a minimum in mid-March (profile 2, Figure 9) at about the same time as the temperature first reaches the surface freezing point in 1996. Similarly, at 302 m R_+ reaches a minimum 1 month later (profile 3, Figure 9) as the water reaches the surface freezing point. At the deepest instrument, R_+ reaches a minimum in early June with no obvious signal in the temperature record (Figure 8). Finally, profile 4 shows R_+ during late winter when a well-mixed water column would normally be assumed. However, in contrast to the winter profiles at the other moorings, the large bottom boundary layer is absent and some stratification must be present below the deepest instrument. The stratification is presumably maintained by the advection of different water masses by the mean southeasterly flow (Figure 2) that is in the opposite direction to mean flow higher in the water column.

[32] Throughout the FR5 time series, changes in ϕ_+ are assumed to correspond with changes in stratification, as observed at FR6. With no available salinity measurements, temperature is used to defined when HSSW is present and therefore if the water column is mixed or stratified. During winter, when the water column is likely to be well mixed, ϕ_+ is around 45° at the upper two instruments; while during summer this can change to between 20° and 100° (Figure 8). These changes occur with the gradual increase in stratification during summer, and with rapid changes associated with the arrival of HSSW at an instrument in early winter. Of the three instruments on this mooring, the upper instrument at 204 m shows the strongest seasonal signal in ϕ_+, which increases during early winter to a maximum of between 90° and 110°. The maximum in ϕ_+ occurs soon after the minimum in R_+ and the arrival of HSSW at the instrument in March. A similar response is also seen a few weeks later at 305 m. Here, the phase changes rapidly with the arrival of HSSW, particularly in April 1995 when ϕ_+ changes from 20° to 100°. This response to the arrival of HSSW is almost identical to the upper instrument at FR6 that was also located just below the draft of the ice shelf. In the subsequent years, this response at 305 m is either weak or absent. At the deepest instrument (551 m), ϕ_+ is highly variable with rapid changes of up to 40°, particularly during the winter of 1996, suggesting that the nearby pycnocline is periodically moving close to the instrument, although there is no corresponding signal in temperature or R_+. A further anomaly occurs in the tidal currents at the deepest instrument. Of all the ice front current data, only FR5 (551 m) has large fluctuations from about 7 cm s^{-1} to 11 cm s^{-1} in R_- (not shown) that coincide principally with the stratified conditions in early 1996. Although the instrument is close to the pycnocline observed in the CTD profile (Figure 3), it is unclear why such changes in phase and amplitude should occur. Nevertheless, these fluctuations in amplitude and phase of the rotary components result in ellipse orientation swings of up to 35° and a doubling of the semimajor axis during periods of stratification. Similar features are also present in the S_2 tidal currents, resulting in peak spring tides with speeds of over 35 cm s^{-1}, while during winter the peak spring tides can fall to less than 20 cm s^{-1}.

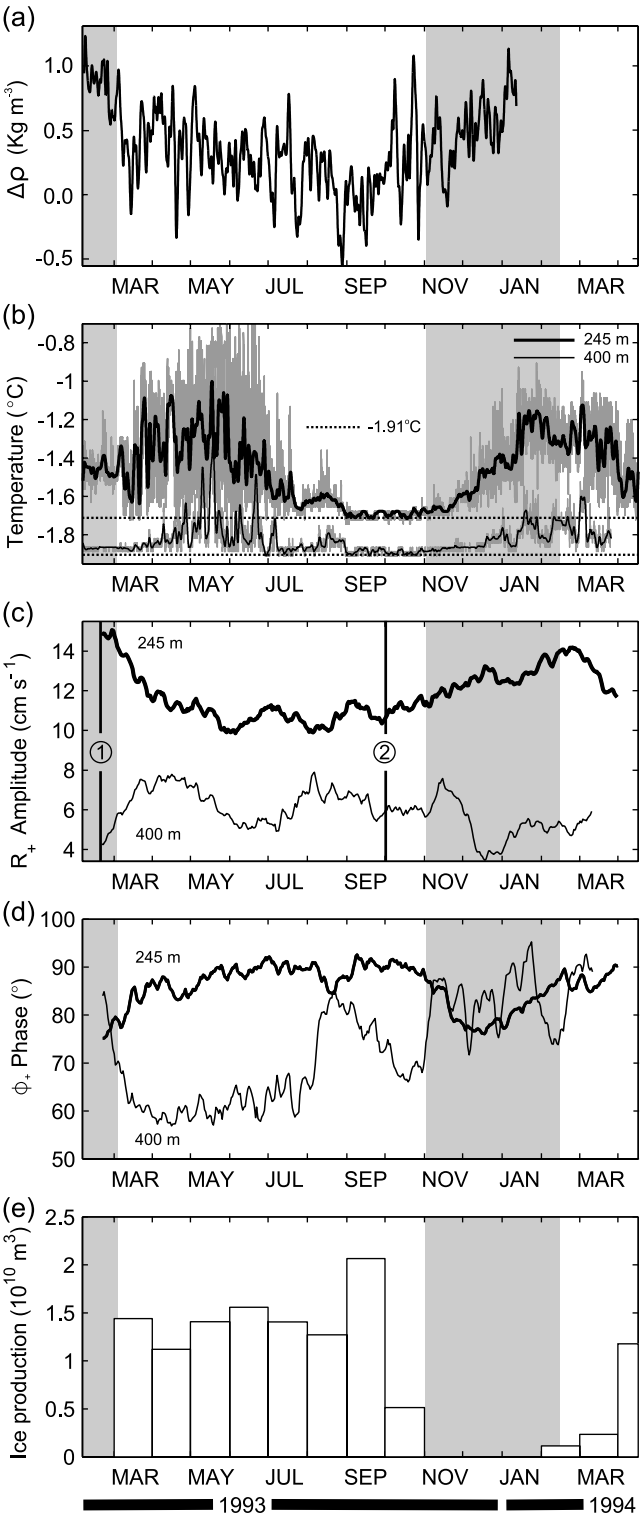

Figure 10. Time series data from mooring R2. (a) Daily averaged seawater density difference ($\Delta\rho$) between the instruments at 400 and 245 m. (b) Raw and daily averaged potential temperature time series data. The data from 245 m have been offset by 0.2°C, and the dotted line shows the surface freezing temperature of −1.91°C. (c) Time series of the anticlockwise rotary component (R_+) for the M_2 tidal constituent. The numbered vertical lines show when R_+ observations are used for the vertical profiles in Figure 11. (d) Time series of the M_2 ϕ_+. (e) Bar chart of sea ice production in the coastal polynya along Ronne Ice Front for each month of the mooring record. The shaded areas in each plot show the summer melting season [*Renfrew et al.*, 2002].

4.3. Mooring R2

[33] Positioned midway along Ronne Ice Front, R2 is clearly influenced by the effects of λ_{crit} and stratification [*Foldvik et al.*, 2001]. During September and October, the water column appears well mixed, as the temperature at both instruments is close to the surface freezing point (Figure 10). An intrusion of MWDW in the mid−water column, which has been observed near the ice front during several summer cruises [e.g., *Foldvik et al.*, 1985; *Gammelsrød et al.*, 1994; *Nicholls et al.*, 2003], results in stratification of the water column between summer and early winter. The mooring had two instruments in the lower half of the water column at 245 m

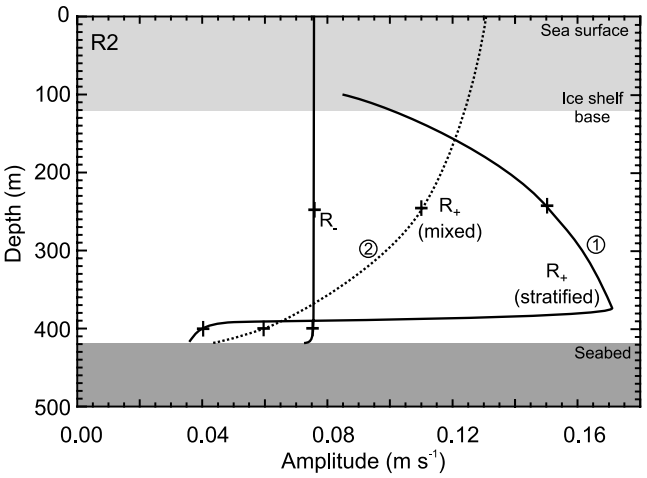

Figure 11. Depth variations of the clockwise (R_-) and anticlockwise (R_+) tidal current components for M_2 at mooring R2. The profile numbers correspond to the numbered vertical lines in Figure 10c, and the crosses are the current meter measurements from those times. The profile lines indicate the conceptual vertical R_+ current profiles for well-mixed (profile 1) and stratified (profile 2) conditions. The light shading indicates the portion of water column occupied by the nearby ice shelf, and the dark shading indicates the seabed.

and 400 m; however, unlike FR5 and FR6, no instruments were deployed close to the depth of the nearby ice shelf base and it is therefore not possible to be certain how the profile of the R_+ changes higher in the water column. At the time of the mooring deployment the nearby CTD profile showed a pycnocline at 380 m, 20 m above the lowest instrument (Figure 3), therefore it is likely that the bottom boundary layer is confined below this pycnocline as observed at FR5.

[34] Focusing on the start of the mooring deployment in Figure 10, R_+ at 400 m increases from 4 cm s^{-1} to 7.5 cm s^{-1}, while at 245 m, R_+ decreases from 15 cm s^{-1} to 11 cm s^{-1} as the contrast in density ($\Delta\rho$) and hence stratification is reduced at the start of the freezing season. This pattern of change in R_+, particularly around 400 m, is comparable to the modeled development of a sub–ice shelf pycnocline at these latitudes [*Makinson*, 2002a]. With a pycnocline close to the seabed, the lower boundary layer is confined below it and frictional forces intensify, reducing R_+. Conversely, erosion of the pycnocline and a decrease in stratification causes the boundary layer and frictional influence to extend over a larger part of the water column and R_+ increases. Hence, as R2 has a similar water column structure to FR5, it is probable that the profile of R_+ during periods of stratification is comparable; with the largest R_+ lower in the water column and a relatively high shear across the pycnocline (profile 1, Figure 11). During the transition from summer to winter conditions, ϕ_+ changes from 75° to 90° at the upper instrument and, rapidly, from 85° to 60° at the lower instrument.

[35] By the end of March, R_+ and ϕ_+ have stabilized. Through March to July, the temperature fluctuates by up to 1.1°C, from −1.8°C to −0.7°C within 1-hour periods at 245 m as the peak temperatures increased until late June. At 400 m, the hourly fluctuations are less pronounced, with changes of not more than 0.3°C being observed. By the end of August, no traces of MWDW are present until its return in late November. During the earlier part of this period, when the water column is well mixed, the largest observed wintertime R_+ at any of the ice front moorings occurs at R2 (245 m). Therefore it is likely that the bottom boundary layer thickness extends throughout the 420 m water column with the largest R_+ located at the surface (profile 2, Figure 11). As the MWDW returns, stratifying the mid–water column, R_+ at 400 m decreases to a minimum during December, presumably as the pycnocline reestablishes above the instrument. Only when this pycnocline goes below the instrument at 400 m, and MWDW is observed during January, does R_+ increase from 4 cm s^{-1} to 5.5 cm s^{-1}. At 245 m, R_+ increases from around 11 cm s^{-1} to 14 cm s^{-1} while ϕ_+ changes from 86° to 76° as MWDW occupies the water column and stratification increases through November after ice production has ceased. During the summer period, ϕ_+ at the lowest instrument shows large fluctuations similar to those observed at FR5 and presumably associated with the nearby pycnocline.

4.4. Mooring FR3

[36] Of the four ice front moorings, FR3 is farthest from $\lambda_{crit}(M_2)$ (2.5° or 280 km to the south). With only one instrument at 203 m, no observational current profiles are possible although the changes can still be seen in temperature, salinity, and the tidal current data (Figure 12). During the summer melting season the water temperature is typically 0.02°C–0.03°C above the freezing point. The melting season is followed by a period, between March and June, when ISW is observed and the mean current flows northwest parallel to the ice front. The most prominent response of the tides is associated with the prolonged ISW event, lasting about 100 days in 1996. R_+ increases from about 6.5 cm s^{-1} to a peak of 12.5 cm s^{-1} in mid-May and ϕ_+ reduces to 70° from a winter mean of around 95°. The rapid decline in R_+ ends soon after mid-June as the water temperature reaches the surface freezing point and the salinity begins to increase, a pattern of response that is also observed at the other ice front moorings. By mid-July, the salinity reaches a plateau and HSSW dominates the water column at the same time as the mean flow slows and reverses direction (not shown). During this period, when the water column is well mixed, it is likely that, because of its relative shallowness, the bottom boundary occupies the entire water column (profile 1, Figure 13). During the early winter periods of 1995 and 1997, observations show almost no ISW is present and there is no response R_+. However, ϕ_+ is reduced by about 10° during these periods, after the 14° yr^{-1} drift in ϕ_+ is accounted for, suggesting the presence of weak stratification.

[37] During periods of stratification, it is not known whether R_+ higher in the water column is reduced as seen at FR5 and FR6. However, if conditions similar to those observed in the CTD profile occur (Figure 3), with a relatively well-mixed water column below the ice shelf draft capped by a sharp pycnocline it is likely that a second boundary layer associated with the ice shelf base would be present (profile 2, Figure 13). For this to happen during the first half of winter, the outflow of ISW must block the descent of HSSW below the draft of the ice shelf, since at FR5 and FR6, HSSW dominates most of the water column by May. Clearly, these conditions must have been met

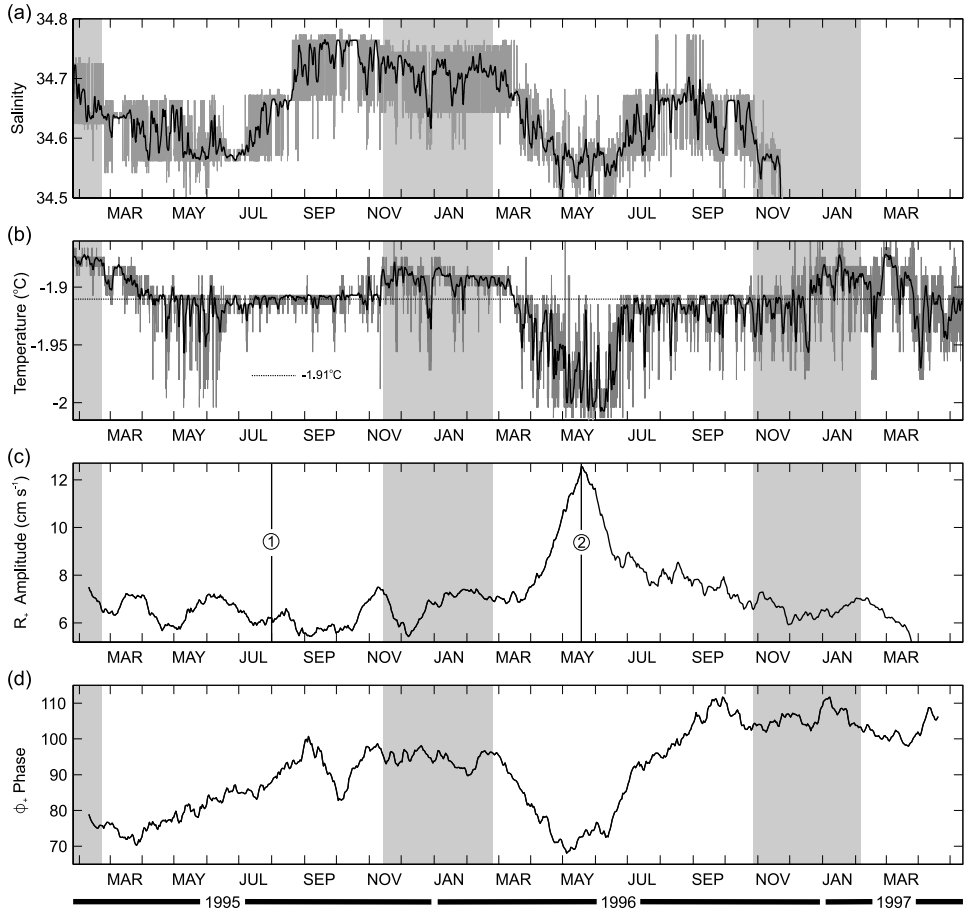

Figure 12. Time series data from the instrument at 203 m on mooring FR3. (a) Raw and daily averaged salinity time series data. (b) Raw and daily averaged potential temperature time series data. The dotted line shows the surface freezing temperature of −1.91°C. (c) Time series of the anticlockwise rotary component (R_+) for the M_2 tidal constituent. The numbered vertical lines show when R_+ observations are used for the vertical profiles in Figure 13. (d) Time series of the M_2 ϕ_+. The shaded areas in each plot show the summer melting season [*Renfrew et al.*, 2002].

during 1996, as ISW in the water column coincides with the large increase in R_+.

4.5. Tidal Advection and Mixing

[38] In addition to the strong seasonal signals in both temperature and salinity, the data from some instruments contain episodes when temperature and salinity exhibit variability on semidiurnal and spring-neap timescales. These signals are confined to the summer and early winter, and are only observed when stratification is present. At semidiurnal timescales, most instruments show some degree of variability, predominantly during spring tides when tidal excursions are greatest. Of the ice front moorings, FR3 exhibits the most persistent semidiurnal signal where the tidal excursion is up to 3.5 km. Here, during the first half of winter, fluctuations of up to 0.1 occur in temperature and to a lesser extent salinity (Figure 12), with colder fresher water at the end of an outflow and warmer saltier water at the end of the inflow, as the water is advected toward and away from the ice shelf cavity. During winter, there are almost no fluctuations in temperature, although salinity retains a weak intermittent signal. The largest temperature fluctuations of up to 1°C occur at R2 (Figure 10), as the water mass at the

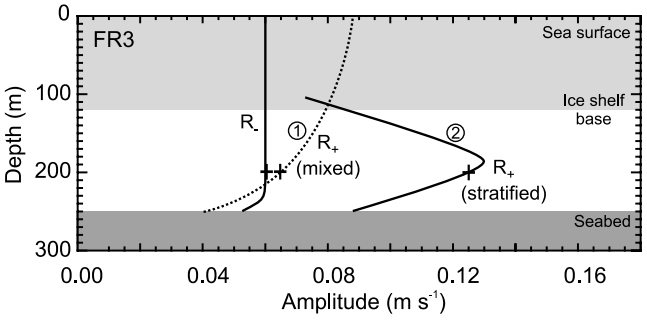

Figure 13. Depth variations of the clockwise (R_-) and anticlockwise (R_+) tidal current components for M_2 at mooring FR3. The profile numbers correspond to the numbered vertical lines in Figure 12c, and the crosses are the current meter measurements from those times. The profile lines indicate the conceptual vertical R_+ current profiles for well-mixed (profile 1) and stratified (profile 2) conditions. The light shading indicates the portion of water column occupied by the nearby ice shelf, and the dark shading indicates the seabed.

upper instrument periodically switches between MWDW and HSSW. However, the inflow and outflow temperature often switches rapidly, suggesting a temperature field that varies nonmonotonically both horizontally and vertically. Some of the instruments have periods of 1 or 2 months, during summer or early winter, when temperature and salinity change on a weekly timescale because of increased mixing during spring tides followed by restratification during neaps. This is most clearly seen in the upper instrument at FR6 in March and April 1996 (Figure 4) where, during spring tides, both the temperature and salinity increase as ISW is mixed with warmer saltier water. During neap tides, the water column restratifies and ISW is reestablished at the instrument.

5. Summary and Conclusions

[39] We have used data obtained at four sites along Ronne Ice Front to reveal how the semidiurnal critical latitude and water column stratification influence the vertical structure of tidal currents. These data show considerable seasonal and interannual variability in both semidiurnal tidal current structure and water column stratification. The primary mechanism driving the water column seasonality is production of HSSW during sea ice formation, eroding stratification, and creating a well-mixed water column. By late winter there has been sufficient HSSW production in the polynya along Ronne Ice Front to ensure that the water column, which ranges from 250 m on Berkner Shelf to just over 600 m in Ronne Depression, is well mixed and dominated by HSSW, although the precise timing depends on the intensity of sea ice formation and advection of water masses within the polynya.

[40] Typically, during this winter period, the disparity between the two rotary boundary layers close to $\lambda_{crit}(M_2)$ is most obvious. The R_- boundary layer lies below the deepest moored instruments and is inferred to be around 10 m thick [*Makinson*, 2002a], while the R_+ boundary layer thickness is observed to be over an order of magnitude greater. At some locations, such as R2 and FR3, the bottom R_+ boundary layer is likely to occupy the entire water column, which at R2 is over 400 m. During this well-mixed winter period, there is generally little variation in any of the tidal rotary components. However, ϕ_- steadily decreases almost linearly by up to $18^\circ\ yr^{-1}$ while ϕ_+ increases annually by approximately an equivalent amount for all the ice front moorings. These observed changes in ϕ_- and ϕ_+, for both diurnal and semidiurnal tides, are most likely the result of Ronne Ice Front advancing toward the moorings.

[41] Within the water column, the onset of stratification at some sites begins in late winter as sea ice formation and HSSW production declines rapidly after September. The initial tidal response occurs in ϕ_+ which is signified by a divergence away from the more uniform winter values as observed, for example, at FR6. By early November, HSSW production has ceased and the summer melting season begins. Temperature and salinity at instruments higher in the water column at FR6 and FR3 begin to respond to these changes. However, it is the appearance of either ISW or MWDW, driven by the larger-scale circulation, which significantly modifies the stratification along the ice front. The precise timing of these events varies between each mooring but the tidal response is synchronized with the changes occurring within the water column. The initial tidal response is in ϕ_+, but with increasing stratification, R_+ responds and amplitudes increase below the draft of the nearby ice shelf base. At some instruments, for example, FR6 (442 m) and FR5 (551 m), R_+ increases by up to 100% and ϕ_+ can change by up to 80° for the M_2 tide, with similar responses in S_2 and N_2, while the water column above the ice shelf draft at FR5 (204 m) detaches from that below and R_+ decreases by up to 70%. In contrast, the clockwise R_- and ϕ_- components together with the diurnal tides remain unaffected by the changes in stratification. These increases in the semidiurnal tidal amplitudes below the draft of the ice shelf, combined with the diurnal tides, can increase the total tidal current amplitude by over 50% at some locations within the water column, yet within the limitations of these sparse observations, the depth averaged current does not appear to change significantly with the seasons.

[42] One surprising feature of the semidiurnal tidal current profiles is the presence of a second boundary layer, which is associated with the nearby ice shelf base. This additional boundary layer gives the impression of an ice covered water column, despite the moorings being several kilometers offshore of the ice front. These two boundary layers occupy the entire water column beneath the draft of the adjacent ice shelf and may extend up to the pycnocline associated with the surface mixed layer. R_+ therefore increases both upward from the seabed, and downward from the depth of the ice shelf base. This increase in R_+ away from the boundaries can on occasion, result in a change in the rotation of the current vector from clockwise near the boundaries to anticlockwise in the mid–water column. Furthermore, these large boundary layers increase the shear within the whole water column enhancing vertical mixing along the ice front region. Beyond the ice front region, the upper boundary layer will presumably decaying with distance from the ice front over some tens of kilometers, before tidal mixing becomes restricted to the bottom boundary layer.

[43] The process of water column cooling and production of HSSW begins with the onset of winter freezing during February. The data clearly show the erosion of stratification as HSSW convects down through the water column. A few weeks after the onset of freezing, while the surface mixed layer is being eroded, the stratification within the body of the water column is at a maximum, leading to a strong tidal response, particularly in R_+, which reaches a peak below the draft of the nearby ice shelf at this time. The recovery of water temperatures to the surface freezing point and the descent of HSSW deeper into the water column, results in a rapid decline in R_+ and changing ϕ_+. The arrival of HSSW and associated pycnocline at individual instruments is observed in the temperature and salinity as well as the tidal response, with minima in R_+ and a rapid change in ϕ_+, signifying the transition from stratified to well-mixed conditions at an instrument.

[44] From these ice front data, a clear picture has emerged showing that semidiurnal tidal currents along the Ronne Ice Front region, and close to $\lambda_{crit}(M_2)$, are considerably amplified below the draft of the ice shelf by the presence of seasonal stratification that controls the level of coupling through the water column. These results are consistent with

boundary layer theory. During periods of stratification, the profile of R_+ (M_2) below the draft of the ice shelf matches both the observations from beneath fixed ice cover in the Arctic [*Prinsenberg and Bennett*, 1989], and the R_+ profiles derived from a tidally driven vertical mixing model applied to the water column beneath FRIS [*Makinson*, 2002a]. Ice front observations such as these highlight the difficulties in interpreting data from short-term moorings and provide insight into how λ_{crit}, stratification and the nearby Ronne Ice Shelf influence tidal current profiles throughout the year. In addition, the observed sensitivity of the M_2 anticlockwise component to changes in stratification along Ronne Ice Front suggests that it is the best indicator for characterizing changes in stratification after direct observations of density variations.

[45] **Acknowledgments.** The authors wish to express their gratitude to the personnel of HMS *Endurance* and *Polarstern* and R/V *Lance* for their support during the cruises. We are also grateful to Keith Nicholls, Robin Robertson, and an anonymous reviewer for their careful reviews of the manuscript and constructive comments.

References

Foldvik, A., T. Gammelsrød, N. Slotsvik, and T. Tørresen (1985), Oceanographic conditions on the Weddell Sea Shelf during the German Antarctic Expedition 1979/80, *Polar Res.*, *3*(2), 209–226.

Foldvik, A., J. H. Middleton, and T. D. Foster (1990), The tides of the southern Weddell Sea, *Deep Sea Res.*, *37*(8), 1345–1362.

Foldvik, A., T. Gammelsrød, E. Nygaard, and S. Østerhus (2001), Current meter measurements near Ronne Ice Shelf, Weddell Sea: Implications for circulation and melting underneath the Filchner-Ronne ice shelves, *J. Geophys. Res.*, *106*(C3), 4463–4477.

Foldvik, A., T. Gammelsrød, S. Østerhus, E. Fahrbach, G. Rohardt, M. Schröder, K. W. Nicholls, L. Padman, and R. A. Woodgate (2004), Ice shelf water overflow and bottom water formation in the southern Weddell Sea, *J. Geophys. Res.*, *109*, C02015, doi:10.1029/2003JC002008.

Foreman, M. G. G. (1977), *Manual for Tidal Currents Analysis and Prediction*, 70 pp., Inst. of Ocean Sci., Patricia Bay, Sidney, B. C., Canada.

Furevik, T., and A. Foldvik (1996), Stability at M_2 critical latitude in the Barents Sea, *J. Geophys. Res.*, *101*(C4), 8823–8837.

Gammelsrød, T., A. Foldvik, O. A. Nøst, Ø. Skagseth, L. G. Anderson, E. Fogelqvist, K. Olsson, T. Tanhua, E. P. Jones, and S. Østerhus (1994), Distribution of water masses on the continental shelf in the southern Weddell Sea, in *The Polar Oceans and Their Role in Shaping the Global Environment*, *Geophys. Monogr. Ser.*, vol. 85, edited by O. M. Johannesen, R. D. Muench, and J. E. Overland, pp. 159–176, AGU, Washington, D. C.

Howarth, M. J. (1998), The effect of stratification on tidal current profiles, *Cont. Shelf Res.*, *18*(11), 1235–1254.

LeBlond, P. H., and L. A. Mysak (1978), *Waves in the Ocean*, 602 pp., Elsevier, New York.

Makinson, K. (2002a), Modeling tidal current profiles and vertical mixing beneath Filchner-Ronne Ice Shelf, Antarctica, *J. Phys. Oceanogr.*, *32*(1), 202–215.

Makinson, K. (2002b), Tidal currents and vertical mixing processes beneath Filchner-Ronne Ice Shelf, Ph.D. thesis, Open Univ., Milton Keynes, U. K.

Makinson, K., and K. W. Nicholls (1999), Modeling tidal currents beneath Filchner-Ronne Ice Shelf and on the adjacent continental shelf: Their effect on mixing and transport, *J. Geophys. Res.*, *104*(C6), 13,449–13,465.

Makinson, K.. and M. Schröder (2004), Ocean processes and seasonal inflow along Ronne Ice Front, in *Forum for Research Into Ice Shelf Processes*, edited by L. H. Smedsrud, *Rep. 15*, pp. 11–16, Bjerknes Cent. for Clim. Res., Bergen, Norway.

Nicholls, K. W., and K. Makinson (1998), Ocean circulation beneath the western Ronne Ice Shelf, as derived from in situ measurements of water currents and properties, in *Ocean, Ice, and Atmosphere: Interactions at the Antarctic Continental Margin*, *Antarct. Res. Ser.*, vol. 75, edited by S. S. Jacobs and R. F. Weiss, pp. 301–318, AGU, Washington, D. C.

Nicholls, K. W., S. Østerhus, K. Makinson, and M. R. Johnson (2001), Oceanographic conditions south of Berkner Island, beneath Filchner-Ronne Ice Shelf, Antarctica, *J. Geophys. Res.*, *106*(C6), 11,481–11,492.

Nicholls, K. W., L. Padman, M. Schröder, R. A. Woodgate, A. Jenkins, and S. Østerhus (2003), Water mass modification over the continental shelf north of Ronne Ice Shelf, Antarctica, *J. Geophys. Res.*, *108*(C8), 3260, doi:10.1029/2002JC001713.

Nøst, E. (1994), Calculating tidal current profiles from vertically integrated models near the critical latitude in the Barents Sea, *J. Geophys. Res.*, *99*(C4), 7885–7901.

Padman, L., H. A. Fricker, R. Coleman, S. Howard, and L. Erofeeva (2002), A new tidal model for the Antarctic ice shelves and seas, *Ann. Glaciol.*, *34*, 247–254.

Pereira, A. F., A. Beckmann, and H. H. Hellmer (2002), Tidal mixing in the southern Weddell Sea: Results from a three-dimensional model, *J. Phys. Oceanogr.*, *32*(7), 2151–2170.

Prandle, D. (1982), The vertical structure of tidal currents, *Geophys. Astrophys. Fluid Dyn.*, *22*(1–2), 29–49.

Prinsenberg, S. J., and E. B. Bennett (1989), Vertical variations of tidal currents in shallow land fast ice-covered regions, *J. Phys. Oceanogr.*, *19*(9), 1268–1278.

Renfrew, I. A., J. C. King, and T. Markus (2002), Coastal polynyas in the southern Weddell Sea: Variability of the surface energy budget, *J. Geophys. Res.*, *107*(C6), 3063, doi:10.1029/2000JC000720.

Robertson, R. (2001a), Internal tides and baroclinicity in the southern Weddell Sea: 1. Model description, *J. Geophys. Res.*, *106*(C11), 27,001–27,016.

Robertson, R. (2001b), Internal tides and baroclinicity in the southern Weddell Sea: 2. Effects of the critical latitude and stratification, *J. Geophys. Res.*, *106*(C11), 27,017–27,034.

Robertson, R. (2005a), Baroclinic and barotropic tides in the Ross Sea, *Antarct. Sci.*, *17*(1), 107–120.

Robertson, R. (2005b), Baroclinic and barotropic tides in the Weddell Sea, *Antarct. Sci.*, *17*(3), 461–474.

Robertson, R., L. Padman, and G. D. Egbert (1998), Tidal currents in the Weddell Sea, in *Ocean, Ice, and Atmosphere: Interactions at the Antarctic Continental Margin*, *Antarct. Res. Ser.*, vol. 75, edited by S. S. Jacobs and R. Weiss, pp. 341–369, AGU, Washington, D. C.

Robertson, R., A. Beckmann, and H. Hellmer (2003), M_2 tidal dynamics in the Ross Sea, *Antarct. Sci.*, *15*(1), 41–46.

Shcherbina, A. Y., L. D. Talley, and D. L. Rudnick (2003), Direct observations of North Pacific ventilation: Brine rejection in the Okhotsk Sea, *Science*, *302*(5652), 1952–1955.

Simpson, J. H., and J. Sharples (1994), Does the Earth's rotation influence the location of the shelf sea fronts?, *J. Geophys. Res.*, *99*(C2), 3315–3319.

Soulsby, R. L. (1983), The bottom boundary layer of the shelf sea, in *Physical Oceanography of Coastal and Shelf Seas*, *Elsevier Oceanogr. Ser.*, vol. 35, edited by B. Johns, pp. 189–226, Elsevier, New York.

Souza, A. J., and J. H. Simpson (1996), The modification of tidal ellipses by stratification in the Rhine ROFI, *Cont. Shelf Res.*, *16*(8), 997–1007.

Vaughan, D. G., J. Sievers, C. S. M. Doake, G. Grikurov, H. Hinze, V. S. Pozdeev, H. Sandhäger, H. W. Schenke, A. Solheim, and F. Thyssen (1994), Map of subglacial and seabed topography, Filchner-Ronne-Schelfeis, Antarktis, scale 1:2,000,000, Inst. für Angew. Geod., Frankfurt am Main, Germany.

Woodgate, R. A., M. Schröder, and S. Østerhus (1998), Moorings from the Filchner Trough and the Ronne Ice Shelf Front: Preliminary tesults, in *Filchner Ronne Ice Shelf Programme Rep. 12*, edited by H. Oerter, pp. 85–90, Alfred Wegener Inst. for Polar and Mar. Res., Bremerhaven, Germany.

K. Makinson, British Antarctic Survey, Natural Environment Research Council, High Cross, Madingley Road, Cambridge CB3 0ET, UK. (kmak@bas.ac.uk)

S. Østerhus, Bjerknes Centre for Climate Research, c/o Geophysical Institute, University of Bergen, Allegaten 70, N-5007 Bergen, Norway. (svein.osterhus@gfi.uib.no)

M. Schröder, Alfred-Wegener-Institut für Polar- und Meeresforschung, Columbusstraße, Postfach 120161, Bremerhaven D-27515, Germany. (mschroeder@awi-bremerhaven.de)